Lawrence Sirovich
Editor

Trends and Perspectives in Applied Mathematics

With 78 Illustrations

Springer-Verlag
New York Berlin Heidelberg London Paris
Tokyo Hong Kong Barcelona Budapest

Contents

Lawrence Sirovich
Division of Applied Mathematics
Brown University
Providence, RI 02912 USA
and
Rockefeller University
New York, NY 10021 USA

Editors

Mathematics Subject Classifications (1991): 01-06, 65Mxx, 76Fxx, 82xx

Library of Congress Cataloging-in-Publication Data
Trends and perspectives in applied mathematics /
[edited by] Lawrence Sirovich.
p. cm. — (Applied mathematical sciences ; v. 100)
Includes bibliographical references.
ISBN 0-387-94201-7 (New York). ISBN 3-540-94201-7 (Berlin).
1. Mathematics. 2. John, Fritz, 1910–. I. Sirovich, L.,
1933–. II. Series: Applied mathematical sciences (Springer-
Verlag New York Inc.) ; v. 100.
QA1.A647 vol. 100
[QA5]
510 s—dc20 93-46063
[510]

Printed on acid-free paper.

Production managed by Hal Henglein; manufacturing supervised by Jacqui Ashri.
Photocomposed copy prepared from a LaTeX file.
Printed and bound by Edwards Brothers, Inc., Ann Arbor, MI.
Printed in the United States of America.

9 8 7 6 5 4 3 2 1

ISBN 0-387-94201-7 Springer-Verlag New York Berlin Heidelberg
ISBN 3-540-94201-7 Springer-Verlag Berlin Heidelberg New York

6

Singularities and Similarities in Interface Flows

Andrea L. Bertozzi, Michael P. Brenner,
Todd F. Dupont, and Leo P. Kadanoff

6.1 Introduction

The onset of singularities in systems of nonlinear partial differential equations is an important issue in fields ranging from general relativity [27], to thermodynamic phase transitions [10], to fluid dynamics [13]. The development of a mathematical singularity, when some quantity associated with the PDE "blows up," reflects the creation of a new structure in the physical system which in turn forces the mathematical formulation to change. Whether or not such singularities are possible for a given system can be a difficult question. A famous problem from the theory of homogeneous incompressible fluids is the question of finite time singularity development in the three-dimensional Navier–Stokes equation: It is unknown if an initially smooth solution can develop a finite time singularity in which the vorticity becomes unbounded [23]. To date, no rigorous proof or counterexample exists; neither numerical nor physical experiments have produced definitive answers [22, 25]. When a particular system allows finite time singularities, many related questions become relevant. For example, do all singularities have universal characteristics, or are there many possible behaviors? Which quantities are unbounded at the singular time?

In this chapter we study these questions for a model equation describing a simple hydrodynamic system that is both easily accessible to experiments and well known to develop singularities in finite time. Consider two different fluids separated by an interface that evolves with dynamics including a pressure jump determined by the Gibbs–Thomson relation

$$\Delta p = \gamma \kappa. \tag{1.1}$$

Here, κ is the mean curvature of the surface, Δp denotes the pressure jump across the interface, and γ is the surface tension of the interface. Whenever the topology of the interface changes, the mean curvature and hence the pressure field develops a singularity. In typical situations, the singularity can also cause the flow velocity to diverge. This type of singularity happens

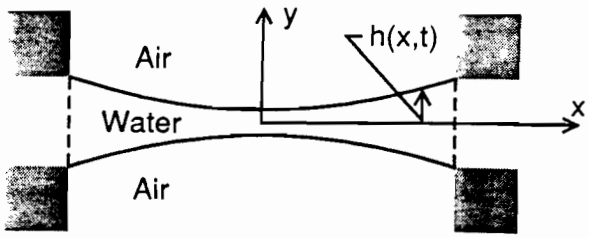

FIGURE 1.1. Picture of the thin neck in a Hele–Shaw environment. This picture is motivated by an experiment [16]. Here, $2h(x,t)$ represents the width of the neck at position x and time t.

Here b is the plate separation, μ is the viscosity, and v is the average horizontal fluid velocity. The xy plane is parallel to the flat surfaces.

We further simplify the problem by considering the evolution of a very thin neck of liquid, such as that of Figure 1.1. We assume the neck is symmetric about the center line $y = 0$ and has a small width $2h(x,t)$ which varies slowly with x. Using the lubrication approximation [7], we assume that the pressure field is independent of y, so that the x component of the velocity, u, is

$$u = -\frac{b^2}{12\mu}\partial_x p \simeq \frac{b^2\gamma}{12\mu}h_{xxx}, \tag{1.4}$$

since in this approximation, $\kappa \simeq h_{xx}$. Finally, the conservation of mass implies that

$$h_t + l_x = 0, \tag{1.5}$$

where $l = uh$ is the current of matter in the x direction. Combining (1.4) and (1.5) we obtain [8, 14, 15]

$$h_t + \frac{b^2\gamma}{12\mu}(hh_{xxx})_x = 0. \tag{1.6}$$

Equation (1.6) involves two approximations: First it assumes that the Reynolds number of the flow is small. This condition might be violated near a singularity. The derivation also assumes that the width of the thin neck $2h$ is much greater than the plate spacing b. When $2h < b$, the dynamics is intrinsically three dimensional and Darcy's law (1.3) does not apply. We point out, however, that in favorable circumstances, equation (1.6) might apply until $h \sim b$. In such a situation the Reynolds number of the flow around the singularity does not become large until the flow is fully three dimensional. For more information see [4].

If we assume that h is independent of y, then the equation depends on only one spatial dimension. We are interested in the case where surface tension dominates the pressure; in particular, we neglect the effect of gravity. The evolution equation for h becomes [17]

$$h_t + \left(\frac{\gamma}{3\mu}(h^3 + Bh)h_{xxx} \right)_x = 0. \tag{1.9}$$

The choice of B depends on conditions at the solid surface. When $h \gg \tilde{h}$, we can take $B = 0$. When the surface is porous, $B = \alpha$, where α is the porosity of the surface [24]. Also of interest are polymeric liquids, which obey the boundary condition $u|_{z=0} = c\partial_z u|_{z=0}$, which yields $B = ch$. Here c is a length scale associated with the polymer [9]. The reader should note that for film thicknesses $h \ll \tilde{h}$, the term Bhh_{xxx} dominates the flux in equation (1.9).

6.1.3 The Model Equation

The examples considered above have a common feature: When h is sufficiently small, the dominant term in the flux has the same functional form, other than the exponent of h. Mathematically, these cases differ only in that the liquid velocity is proportional to h_{xxx} (Hele–Shaw and liquid on porous medium) , hh_{xxx} (polymeric liquids), and h^2h_{xxx} (macroscopic thin film). The velocities all have the general form

$$u \sim h^{n-1}h_{xxx}. \tag{1.10}$$

In nondimensional form, neglecting the terms with higher powers of h, the evolution equation is

$$h_t + (h^n h_{xxx})_x = 0. \tag{1.11}$$

We note that equations of this general form with $1 \leq n \leq 2$ also appear in the literature as slip models for modeling motion near contact lines [19, 26].

We now ask the following questions: Does equation (1.11) allow h to go to zero in finite time? Does this answer depend on on the exponent n? We will show that the value of n determines whether such singularities are possible. There are several transitions in allowable behavior as n varies, some of which are in the range corresponding to the physical models.

Mathematical Background of the Model Equation

The model equation is a fourth-order parabolic equation. The degeneracy of the equation as $h \to 0$ requires h to be bounded away from zero for standard parabolic theory to ensure well-posedness. In this work we consider equation (1.11) as an initial value problem on the bounded domain $[-1, 1]$. In general, one can use either periodic boundary conditions on the interval

[3]. We continue this process in time until $h(x,t)$ hits zero for some value of x. Notice that finite time $h \to \infty$ type singularities are impossible for many of the boundary conditions. On any finite time interval, with either the boundary conditions (1.12), (1.14), or periodic boundary conditions, $\|h_x(\cdot,t)\|_{L^2[-1,1]}$ is an a priori bounded quantity on any time interval $[0,T]$ which forbids h to become unbounded in finite time.

Existence and Behavior of Singularities

We ask whether it is possible for $h \to 0$ either in finite or infinite time. Clearly boundary conditions play an important role. For example, in the case of the "pressure" boundary conditions (1.12), h definitely goes to zero if $p > 2$; the issue is whether it happens in finite or infinite time (see below). Moreover, for the current boundary conditions, a finite time singularity *always* occurs; the issue is whether it occurs on the boundary or in the interior.

We begin by noting that for $n \geq 1$ if $h \to 0$, then necessarily $\int_0^{t_c} |h_{xxxx}|_{L^\infty} dt$ must blow up. We present a formal argument that can be made rigorous:

$$\begin{aligned}
\frac{d}{dt}(h_{min}(t)) &= \frac{d}{dt}(min_x(h(x,t))) = \frac{d}{dt}(h(x_{min},t)) \\
&= h_t(x_{min},t) + h_x(x_{min},t)\dot{x}_{min} \\
&= h_t(x_{min},t) = -h^n h_{xxxx}(x_{min},t) - nh^{n-1}h_{xxx}h_x(x_{min,t}) \\
&= -h_{min}(t)^n h_{xxxx}(x_{min},t).
\end{aligned}$$

Hence, for $n \geq 1$, $h_{min}(t)$ can only go to zero in finite time if $\int_0^{t_c} h_{xxxx}\,(x_{min},t)dt$, and, hence, h_{xxxx}, diverges. Here we use the fact that $h_x(x_{min},t) = 0$.

We now show a result that rules out finite time singularities for some values of n. Furthermore, we include additional results that rule out finite time singularities when h_{xx} is bounded; we observe that this bound holds in many (but not all) of our simulations. We remark that our numerical simulations indicate that the bounds on n presented here may not be sharp. See Section 6.3 for more details.

Theorem 6.1.1 *Let h be a solution to (1.11) with either periodic boundary conditions or (1.14) and smooth initial data $h_0(x) > 0$. Then (1) if $n \geq 3.5$, then there exists a unique smooth solution $h(x,t)$ for all time that satisfies $h(x,t) > 0$. (2) If $n \geq 2$, then the above is true, provided that $h_{xx}(x,t)$ remains bounded.*

The proof is an extension of the one found in [3] showing (1) to be true for $n \geq 4$. We omit some details that are identical to those found in [3]. First consider the case of periodic or (1.14) boundary conditions. We first note that $\int h_x^2$ is an energy function because integration by parts

$$\begin{aligned} w_\infty(x) &= 0, \quad |x| < x_c, \\ w_\infty(x) &= \frac{p}{2}(|x| - x_c)^2, \quad 1 \geq |x| \geq x_c, \\ x_c &= 1 - \sqrt{2/p}. \end{aligned} \tag{1.18}$$

This weak solution has a jump in its second derivative at $\pm x_c$ and hence will produce a singularity in h if $h \to w_\infty(x)$ in infinite time. Thus, when $p > 2$, we always expect a singularity to form, either in finite or infinite time. The details of the infinite time case with $n = 1$ are presented in [8, 11, 28].

When $p < 2$, there need not be a singularity, since the solution can tend toward the positive solution $h_\infty(x)$. However, we cannot rigorously rule out the possibility of finite time singularities for the constant pressure boundary conditions with $n < 4$. This result follows from an extension of Theorem 1.1. First we integrate by parts to see that $\int \varphi_x^2$ is a priori bounded where $\varphi = h - h_\infty$, which, in turn, gives an a priori bound for $\int h_x^2$ and from the boundary conditions, a bound for $\int h$. A calculation shows that

$$\frac{d}{dt}\left[\int h^{2-n} + (n-2)\int h\right] = \frac{d}{dt}[H_n(h)\Big] = -(n-2)(n-1)\int (h_{xx}^2 - p h_{xx})dx.$$

For $n \geq 2$ this time derivative is bounded from above by the constant $(n-2)(n-1)p^2/2$. Hence, finite time singularities are impossible for $n \geq 4$. Note that this bound is higher than the bound of $n \geq 3.5$ for the boundary conditions of Theorem 1.1. The boundary conditions (1.12) provide extra boundary terms that we cannot control as in the a priori estimates used for proving Theorem 1.1. However, we can show part (2) of Theorem 1.1. The bound on $\int h$ gives a bound on $\int_0^T (h_{xxx}(1) - h_{xxx}(-1))dt$ and knowing that h_{xx} is a priori bounded gives definite bounds on $\int_0^T [h_x^3(1) - h_x^3(-1)]$ and $\int_0^T [h_x(1) - h_x(-1)]$. Using these facts, we can bound all of the boundary terms in the dG/dt integral to show that G is a priori bounded on any time interval and produce the following:

Corollary 6.1.1 *Let h be a solution to (1.11) with boundary conditions (1.12) and smooth initial data $h_0(x) > 0$. If $p > 2$, then h will go to zero in either finite or infinite time. If (1) $n \geq 4$, then finite time singularities are impossible and h hits zero in infinite time. If (2) $n \geq 2$, the above is true providing that h_{xx} remains bounded.*

If we consider the "current" (1.13) boundary conditions, we force a finite time singularity to happen and the question becomes one of whether or not it happens on the boundary or in the interior. We have the following:

Theorem 6.1.2 *Let h be a solution to (1.11) with boundary conditions (1.13) and smooth initial data $h_0(x) > 0$. (1) If $n \geq 3.5$ then $h(x,t)$ goes to zero in finite time with the singularity occurring on the boundary of*

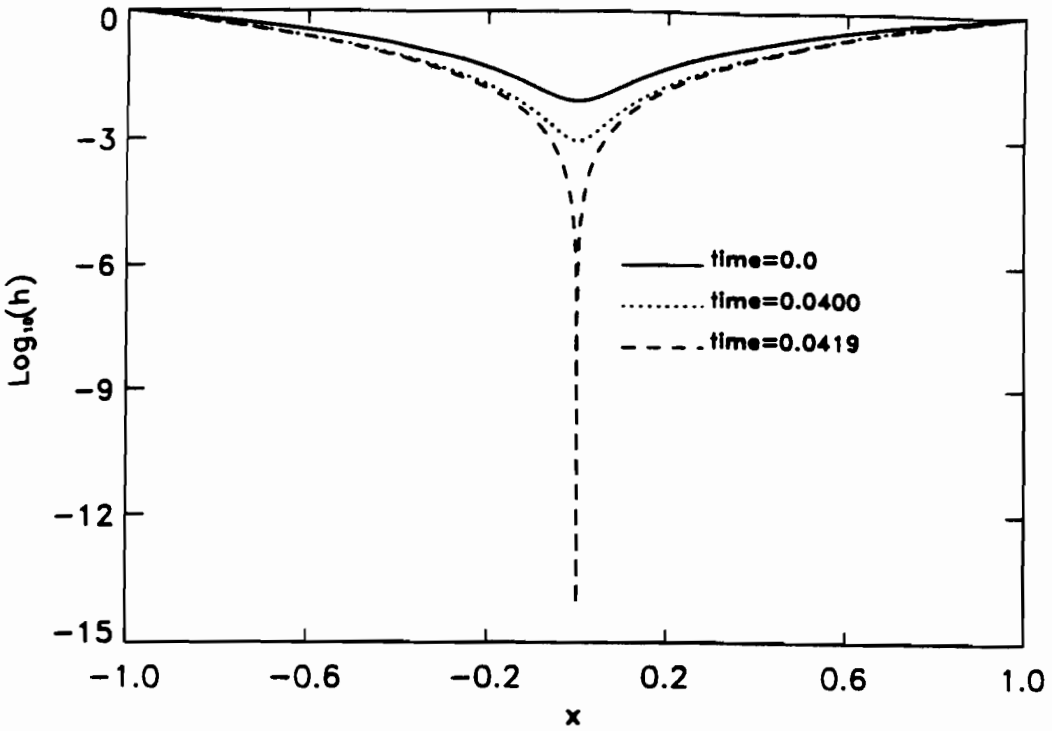

FIGURE 1.3. Finite time singularities at the center of the computational domain for $n = 0.75$. We show a log-linear plot of $h(x,t)$ for successive times before the singularity. Initial conditions and boundary conditions for this solution are detailed in Section 6.3.

(1.12) pressure BC
(1.13) current BC

TABLE 1. Singularities seen in simulations.

case	time	type of touchdown	boundary condition	observed for
i	finite	symmetrical	(1.12)	$0 \le n < 1$
ii	finite	asymmetrical	(1.12) and (1.13)	$0.75 \lesssim n \lesssim 1.2$
iii	infinite	asymmetrical	(1.12)	$0.75 \lesssim n \le \infty$
iv	infinite	symmetrical	(1.12), $p = 2$	$0.75 \lesssim n \le \infty$
v	finite	boundary	(1.13)	$n \gtrsim 2$
vi	infinite	boundary	(1.13)	not observed

In Figures 1.3–1.6, we show typical simulation results illustrating the behaviors of Table 1. Figure 1.3 shows case (i). Here, h goes to zero at $x = 0$ ($n = 0.75$). Figure 1.4 shows case (ii). Here, h becomes small at two nonzero values of x ($n = 1.1$). Figure 1.5 shows case (v), in which a singularity occurs at the boundary of the computational domain ($n = 2.5$). Finally, Figure 1.6 shows case (iii). Here, h remains positive for all time but develops a zero at infinite time ($n = 2.0$). The zero actually develops in the entire interval $[-x_c, x_c]$. Case (iv) is a special case of (iii). Here the fact that $p = 2$ causes the singularity to be symmetric about the minimum,

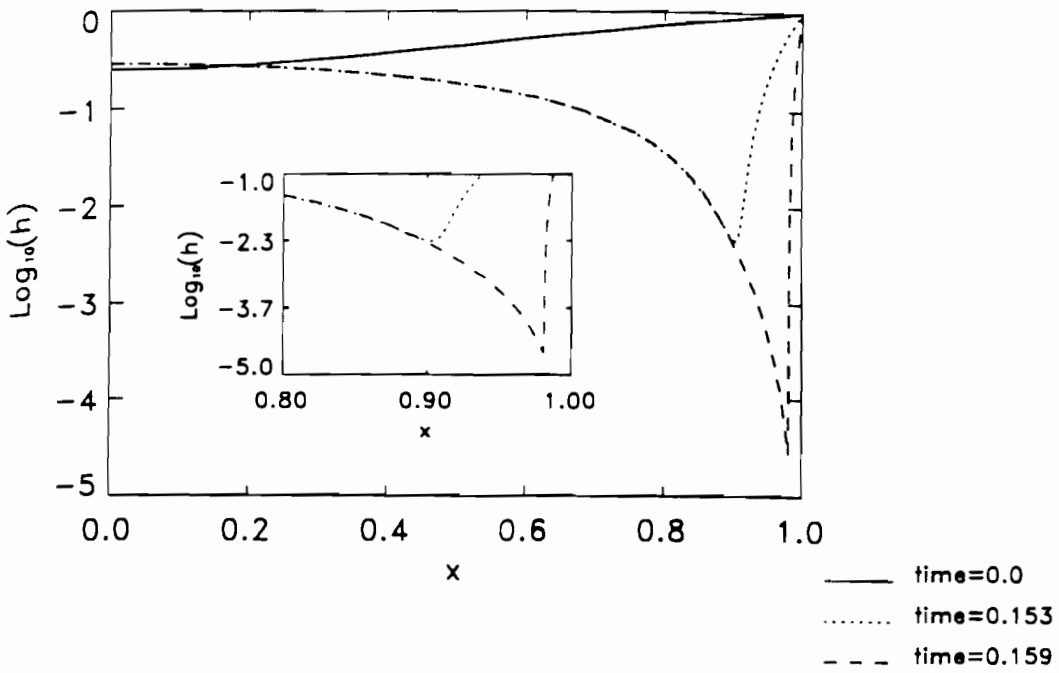

FIGURE 1.5. Finite time singularity at the edge of the simulation region for $n = 2.5$. We show a log-linear plot of $h(x,t)$ versus x for successive times before the singularity. Initial conditions and boundary conditions for this solution are detailed in Section 6.3. The inset shows a blow-up near the singularity.

that is, h has the form

$$h(x,t) = \tau(t)H(\eta), \quad \eta = \frac{x - x_p(t)}{\tau(t)^q}. \tag{1.19}$$

Here, $x_p(t)$ is the position of the minimum of h, and $\tau(t)$ is a time-dependent length scale which describes the size of the region over which the singularity occurs. A singularity happens when $\tau \to 0$. We can obtain an ODE for the shape of H by substituting (1.19) into the evolution equation and making certain assumptions about the relative size of the time-dependent terms in the equation, based on the observed behavior. We must then be able to match the similarity solution, H, at large values of η to a solution in an outer region or to boundary conditions. The matching condition puts a rather severe constraint on the types of similarity solutions that are admissible. In many of the cases described in Table 1, the matching conditions break down at specific values of n, explaining the transitions in the numerical solutions of the PDE.

In the rest of this chapter we explore the link between similarity solutions of the type (1.19) and formation of singularities in the model equation. In the next section, we discuss several classes of similarity solutions, delineated

In order for a similarity solution to describe the region around a singularity, the solution must satisfy the following conditions:

(a) $\tau(t) \to 0$ as $t \to t_c$, the singular time.

(b) $H(\eta)$ is well behaved at large values of η, in order to match H to the outer solution or boundary conditions.

(c) $H(\eta) > 0$.

There are not always solutions which satisfy all of these conditions simultaneously. In particular, Theorem 1.1 indicates that solutions which satisfy (a) through (c) for finite t_c and $x_p \in (-1, 1)$ do not exist when $n > 3.5$. In this section, we analyze the types of similarity solutions of equation (2.1) and determine the values of n for which solutions satisfying the above conditions exist.

Moreover, in our simulations, for certain boundary conditions and values of n, we observe finite time singularities which do not have the simple scaling form (2.2). By determining when a self-similar singularity is *not* possible for a system that allows for finite time singularities, we hope to gain some insight into the development of such complex singularities. We address this issue in Section 6.4.

Similarity solutions are useful for describing more than just the region around a finite time singularity. We observe self-similar solutions, typically with compact support, in other parts of the solution. Another goal of this section is to analyze the existence of these "soliton" solutions. These solutions play an important role in some of the singularity mechanisms described in Section 6.3.

6.2.1 *Derivation of Similarity Solutions*

Substituting the form (2.2) into the basic equation (2.1) gives

$$\frac{\tau_t}{\tau}(1 - q\eta\partial_\eta)H - \frac{\dot{x_p}}{\tau^q}H_\eta + \tau^{n-4q}(H^n H_{\eta\eta\eta})_\eta = 0. \tag{2.3}$$

We classify self-similar solutions by assuming that, to leading order, τ and x_p have power law behavior in $t_c - t$ and then choosing relative sizes of $\dot{\tau}$, $\dot{x_p}$, and τ^{n-4q}. We emphasize that by "similarity solution" we refer merely to solutions which exhibit scaling. In some cases this scaling will yield an exact solution to (2.1). However, in most instances, the scaling gives an approximate solution that only solves (2.1) to leading order in a small variable (usually τ or a power of τ). We classify these different types of similarity solutions by the relative sizes of the time-dependent coefficients in equation (2.3).

q Equation

One possibility is that all the terms in (2.3) are of the same order of magnitude when η is of order unity. In that case, $x_p = \alpha\tau^q$, so that x_p can be

two undefined "critical indices": We know neither the value of q nor the time dependence of τ. In general, matching conditions fixes these indices. In Section 6.3, we show that the velocity equation is relevant for understanding case (v) of Table 1, touchdown on the boundary.

Current Equation

A third possibility is that the time derivative h_t [the first two terms in (2.3)] is negligible, so that

$$\begin{aligned} |\dot{x_p}| &\ll \tau^{n-3q}, \\ |\tau_t| &\ll \tau^{n-3q}. \end{aligned} \tag{2.11}$$

In this case, H obeys

$$(H^n H_{\eta\eta\eta})_\eta = 0. \tag{2.12}$$

If the constant of integration, denoted by λ, is positive, we have

$$H^n H_{\eta\eta\eta} = \lambda. \tag{2.13}$$

This equation expresses the fact that the *current* is independent of position near the singularity. Note that again the similarity solution does not fix either q, or the time dependence of τ. In Section 6.3, we show that this similarity equation applies near the singularity in several different situations, including cases (ii) and (iii) of Table 1.

Parabolic Equation

We can also consider a case where the time dependences obey (2.11) but the constant of integration in (2.13) is zero. Then, H obeys

$$H_{\eta\eta\eta} = 0. \tag{2.14}$$

We call this the parabolic equation, for, in general, H is a quadratic function of η. In Section 6.3 we show that this solution is applicable in the central and outer regions of case (iii), and in the pinch region of case (i).

Table 2 summarizes similarity solutions we observe in the simulations. Here x_0 is the position in $[0,1]$ where the singularity occurs. Since our simulations are symmetric about 0, we see an identical singularity at $-x_0$. Section 6.3 contains detailed analysis of the connections between the simulations and the similarity solutions.

TABLE 2. Similarity solutions seen in simulations.

location of singularity	time	observed for	pinch region equation	center region equation
$x_0 = 0$	finite	$0 \le n \le 1$	parabolic	same
$0 < x_0 < 1$	finite	$0.75 \lesssim n \lesssim 1.2$	current	not self–similar
$0 < x_0 < 1$	infinite	$0.75 \lesssim n \le 2$	current	q equation, $q = 0$
$0 < x_0 < 1$	infinite	$2 < n < \infty$	current	parabolic
boundary	finite	$n \gtrsim 2$	velocity	not self–similar

A similar analysis holds for the velocity equation (2.10). Tables 4 through 6 summarize the results of the three possible cases $b = 0$, $b < 0$, and $b > 0$.

In Table 5, we present the possible behaviors for the velocity equation with $b > 0$. In Table 6, we present the possible behavior of the velocity equation with $b < 0$.

TABLE 3. Current equation (2.13) behavior.

	$0 \le n \le 1/2$	$1/2 < n < 2$	$2 \le n$
possible zeros	S ($\eta > 0$),**L**,**Q**	S ($\eta < 0$),**L**	**S** ($\eta > 0$)
possible infinities	**S** ($\eta > 0$)	S ($\eta < 0$),**Q**	S ($\eta > 0$),L,**Q**
soliton	possible	possible	not possible
global	not possible	possible	possible
zero only on left	possible	possible	possible
zero only on right	not possible	possible	not possible

TABLE 4. Velocity equation (2.10) with $b = 0$.

	$0 < n < 3/2$	$3/ < n < 3$	$3 \le n$
possible zeros	S ($\eta > 0$),**L**,**Q**	S ($\eta < 0$),**L**	**S** ($\eta > 0$)
possible infinities	**S** ($\eta > 0$)	S ($\eta < 0$),**Q**	S ($\eta > 0$),L,**Q**
soliton	possible	possible	not possible
global	not possible	possible	possible
zero only on left	possible	possible	possible
zero only on right	not possible	possible	not possible

6.3 Simulation Results Compared with Similarity Solutions

6.3.1 Numerical Method

Our numerical scheme is an adaptation of a code described previously in [11]. Thus, some of the language here comes, with permission of the authors, from this source. The simulations use a conventional finite-difference method. The code is an implicit, two-level scheme based on central differences. We also use a dynamically adaptive mesh composed of a fixed macrogrid and adaptive microgrid for higher resolution of singularities. In certain instances, we use a multilevel microgrid for extremely fine resolution of singularities. The finite-difference scheme is essentially identical to the scheme used in [8, 11, 28]. They compared their results to simulation results obtained from a finite element method and found excellent agreement. The new features in the code are the incorporation of "current" boundary conditions (1.13), and a dynamically adaptive multilevel mesh for resolution of moving singularities.

We consider solutions to (1.11) that are symmetric about $x = 0$. Given an initial condition satisfying $h(x,0) = h(-x,0)$, the solution retains this symmetry. Thus, we can solve the equation on the interval $[0,1]$, discretized by the N mesh points,

$$0 = x_1 < x_2 < \cdots < x_N = 1.$$

At each computational time, the arrays h_i and p_i, $i \in [1,...,N]$, approximate $h(x,t)$ and $-h_{xx}(x,t)$, and v_j, $j \in [1,...,N-1]$ approximates $h_{xxx}(x,t)$. The h_i and p_i values exist at the point x_i, and v_i is the computed third derivative at the center of the interval, $(x_i + x_{i+1})/2$. The following picture depicts these associations:

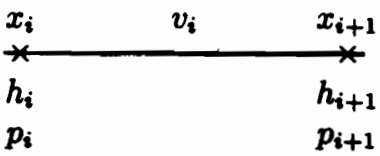

We use the notation

$$\begin{aligned}
\Delta x_{i+1/2} &= x_{i+1} - x_i, \\
x_{i+1/2} &= \tfrac{1}{2}(x_{i+1} + x_i), \\
\Delta x_i &= x_{i+1/2} - x_{i-1/2}, \\
h_{i+1/2} &= \tfrac{1}{2}(h_{i+1} + h_i), \\
\partial h_{i+1/2} &= (h_{i+1} - h_i)/\Delta x_{i+1/2}, \\
\delta^2 h_i &= (\partial h_{i+1/2} - \partial h_{i-1/2})/\Delta x_i.
\end{aligned} \tag{3.1}$$

For simplicity we describe the difference scheme in space first and later indicate the time step process. We replace the equation in (1.11) by:

$$(h_i)_t + (h^n_{i+1/2} v_i - h^n_{i-1/2} v_{i-1})/\Delta x_i = 0, \tag{3.2}$$

$$v_i + \partial p_{i+1/2} = 0, \tag{3.3}$$

$$p_i + \delta^2 h_i = 0. \tag{3.4}$$

We impose the "pressure" boundary conditions by setting $h_N = 1$ and $p_N = -p$ and using the symmetry at $x = 0$. We impose the "current" boundary conditions by setting $v_N = c$, which actually fixes h_{xxx} half of a mesh point away from the boundary instead of on the boundary. This can potentially lead to numerical errors when the solution touches down on the boundary. We cut down the error by dynamically refining the mesh on the boundary as the singularity progresses. This adjustment is both effective and computationally inexpensive.

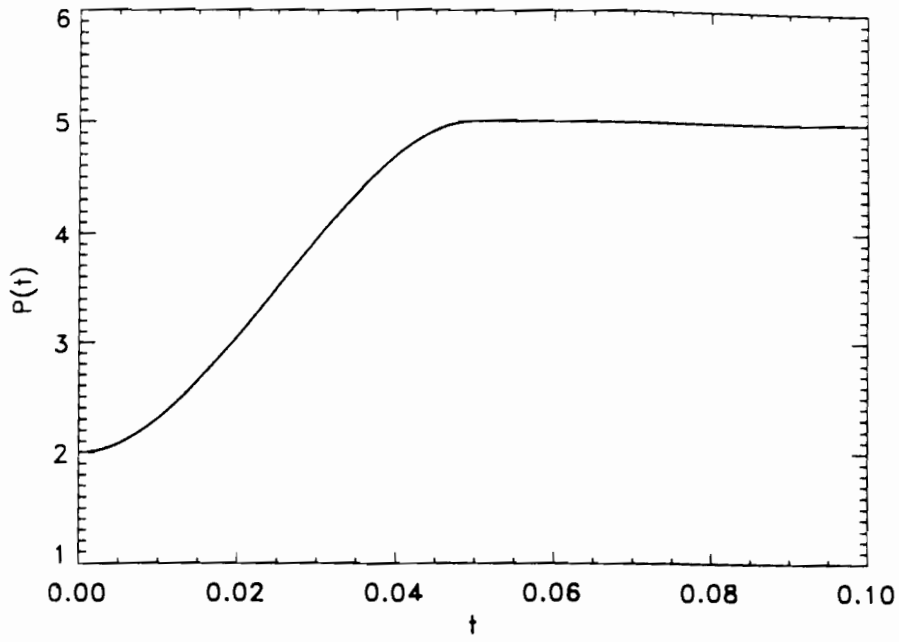

FIGURE 3.1. Typical profile of the boundary pressure as a function of time used in the pressure boundary conditions. We vary the value of the pressure at $t = 0$, and also the rate of increase.

realizable. In the case of the "pressure" boundary conditions, we start with a boundary pressure $p = 2 - \epsilon$, and choose the initial data to be the static parabola corresponding to this pressure

$$h(x,0) = \frac{\epsilon}{2} + \frac{(2-\epsilon)}{2}x^2. \tag{3.5}$$

From this initial state we increase the pressure to some fixed value p. We can then consider the "initial condition" to be the state at the instant $h_{xx}(\pm 1)$ reaches its final fixed value. Figure 3.1 shows a typical graph of the boundary pressure as a function of time. We usually set the maximum p to be 5. The initial conditions thus have essentially two parameters: ϵ and the rate r at which the pressure on the boundary increases. Both of these parameters are relevant; varying either can influence the type of singularity produced.

For the current boundary conditions, we prepare the initial state by starting out with a static parabola at a pressure $p = 2 - \epsilon$ and a boundary current of zero. We then gradually increase the boundary current to its constant final value.

We now present self-similar solutions which accurately describe the approach to zero in the central region and the pinch region. Constantin et al. [8] carried out this analysis in great detail for the case $n = 1$; we extend their results to general n. In the central region, h approaches a similarity solution of the form $h(x,t) = h_0(t)C(x)$, where $C(\pm x_c) = 0$. There are two possible solutions of this type. The first possibility is that h is a solution to the q equation of Section 6.2. The only q equation that can describe the central region has $q = 0$, for when $q \neq 0$, the solutions do not have fixed support. The $q = 0$ solution satisfies

$$h_0(t) = \frac{\lambda}{n} t^{-1/n}$$

with

$$\lambda C = (C^n C_{xxx})_x \tag{3.8}$$

and

$$C(\pm x_c) = 0.$$

In the language of Section 6.2, C must be a soliton solution. As shown there, this type of solution only exists for $n \leq 2$. An alternative in the central region is the parabolic solution

$$h(x,t) = h_0(t)\left(1 - \frac{x^2}{x_c^2}\right). \tag{3.9}$$

This type of solution potentially applies to all values of n. However, it will turn out that it is only possible to match this central region solution onto the pinch region for $n > 2$. Note that the time dependence $h_0(t)$ is not fixed in this case but is determined by the matching. In both cases, $h_0(t)$ goes to zero as t goes to infinity. The solution thus asymptotically approaches the weak solution $w_\infty(x)$ in the central region.

Before proceeding to the pinch region, we check that the numerical solutions agree with the central region solutions. In Figure 3.2 we plot $h(x,t)/h(0,t)$ versus x for $n = 0.9$. We show data for five different times. The above theory predicts that the data should collapse onto a single curve. The solid line in the figure is a solution to equation (3.8) with the initial conditions $C(0) = 1$, $C_\eta(0) = 0$, $C_{\eta\eta}(0) = -2.95$, and $\lambda = 8.40$. The agreement is excellent. In Figure 3.3 we show a similar plot for $n = 3$. Again the data collapse and agree with the parabola (3.9).

Now we consider the solution in the pinch region. We focus on the pinch region near $+x_c$. (The same analysis holds near $-x_c$.) Here, we argue that h approaches a similarity solution

$$h(x,t) = h_{min}(t)H(\eta), \qquad \eta = \frac{x - x_c}{\xi(t)}, \tag{3.10}$$

where H obeys the current equation. The solution matches onto the central region as $\eta \to -\infty$ and onto the outer region as $\eta \to \infty$. The match onto

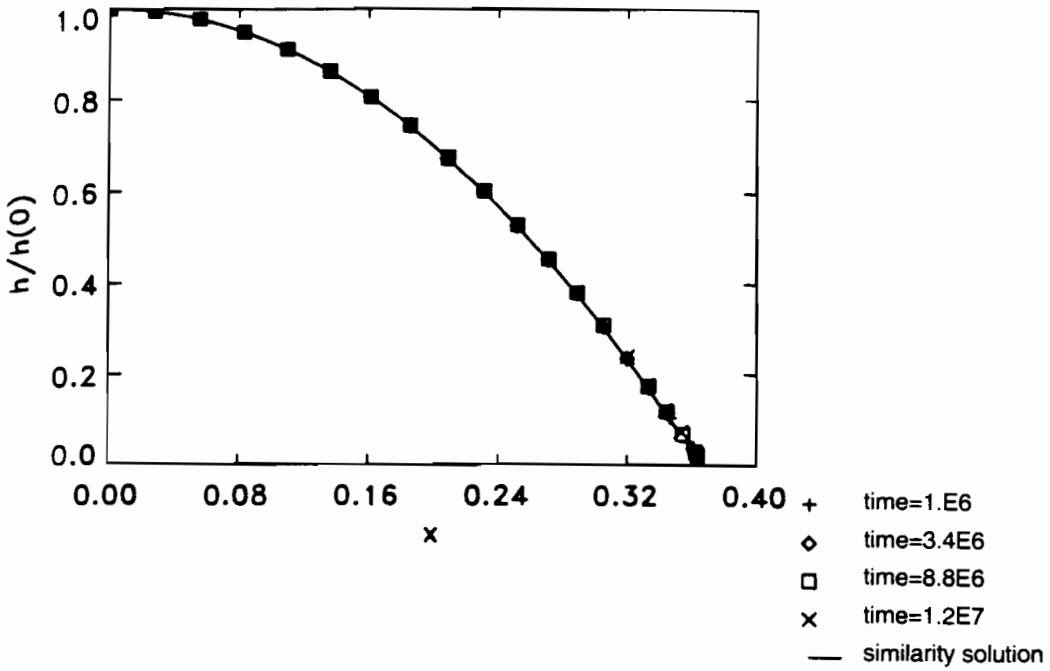

FIGURE 3.3. Rescaled profiles for the central region for $n = 3.0$. Each different symbol represents a numerical solution for a different time. The solid line is a solution to the similarity equation (3.9).

Combining these two results yields

$$h_0(t)^n \sim t\xi^{2n-1}. \tag{3.12}$$

Thus, $h_0(t)$ determines $\xi(t)$. For $1/2 < n < 2$, (3.8) gives

$$h_0 \sim t^{-1/n} \qquad (1/2 < n < 2).$$

For the parabolic solution, the time dependence is fixed by the matching: Near x_c, the edge of the central region, $h(x,t) \approx h_0(t)(x_c - x)$. This means that the solution in the pinch region must have the asymptotic behavior $H(\eta) \sim A\eta$ as $\eta \to -\infty$. From Table 3 of Section 6.2 this asymptotic behavior is only possible for $n > 2$. The match also requires the time dependences agree, so that

$$h_0(t) \sim \xi(t) \qquad (n > 2). \tag{3.13}$$

Combining these results, we find that $h_0(t)$ and $h_{min}(t)$ have the time dependences

$$h_0(t) \sim t^{-p(n)}, \quad h_{min}(t) \sim t^{-q(n)}. \tag{3.14}$$

For $1/2 < n < 2$, the exponents are

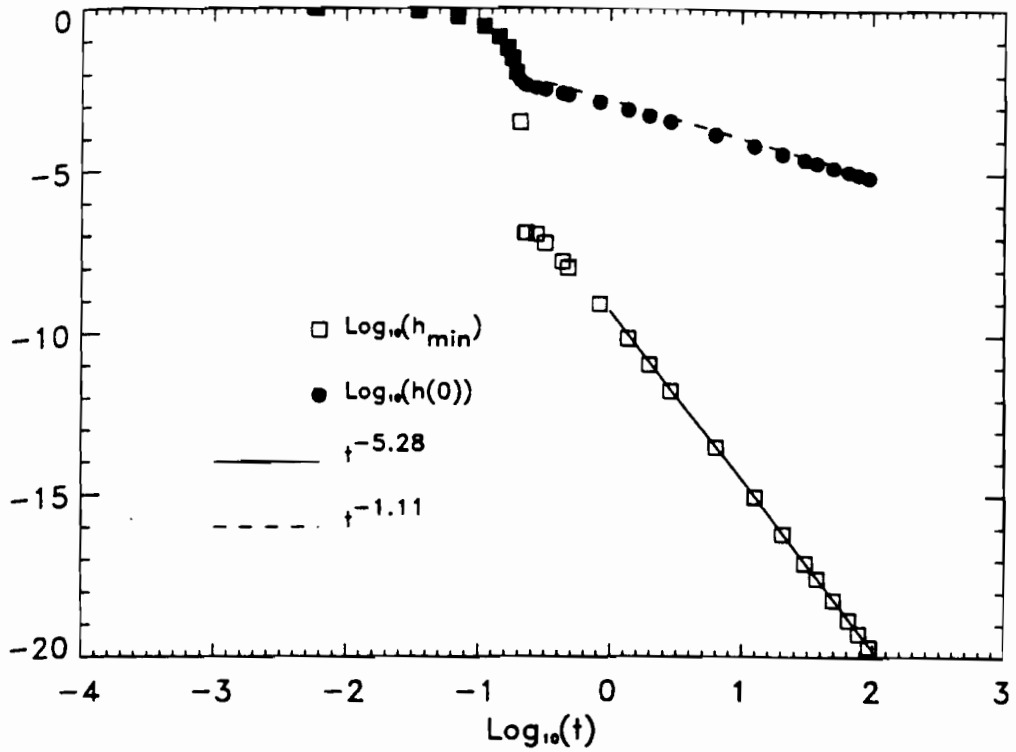

FIGURE 3.5. Time dependences of the minimum height, h_{min}, and the height $h(0,t)$ for $n = 0.9$. The solid and dashed lines are the predictions of the theory.

6.3.3 *Finite Time Singularities at* $\pm x_0$, $0 < |x_0| < 1$

The analysis of the preceding section is simplified by the fact that the singular point does not propagate. In this section we describe a *finite time* singularity in which the singular point does propagate. Dupont et al. [11] and Zhou [28] first discovered and analyzed this singularity in the case $n = 1$, using initial data with $(r, \epsilon) \approx (100, 1/64)$.

The singularity has the same overall structure as the previous infinite time case: There is a pinch region, a central region and an outer region. As before, we model the solution in the pinch region by a similarity solution of the form

$$h(x,t) \approx h_{min}(t) H(\eta), \qquad \eta = \frac{x - x_p(t)}{\xi(t)}, \tag{3.16}$$

where H obeys the current equation with current

$$J(t) = \frac{h_{min}(t)^{n+1}}{\xi(t)^3} \sqrt{} \tag{3.17}$$

and the pinch point $x_p(t)$ is a linear function of time as $t \to t_c$. However, in contrast to the infinite time singularities, the central region and outer

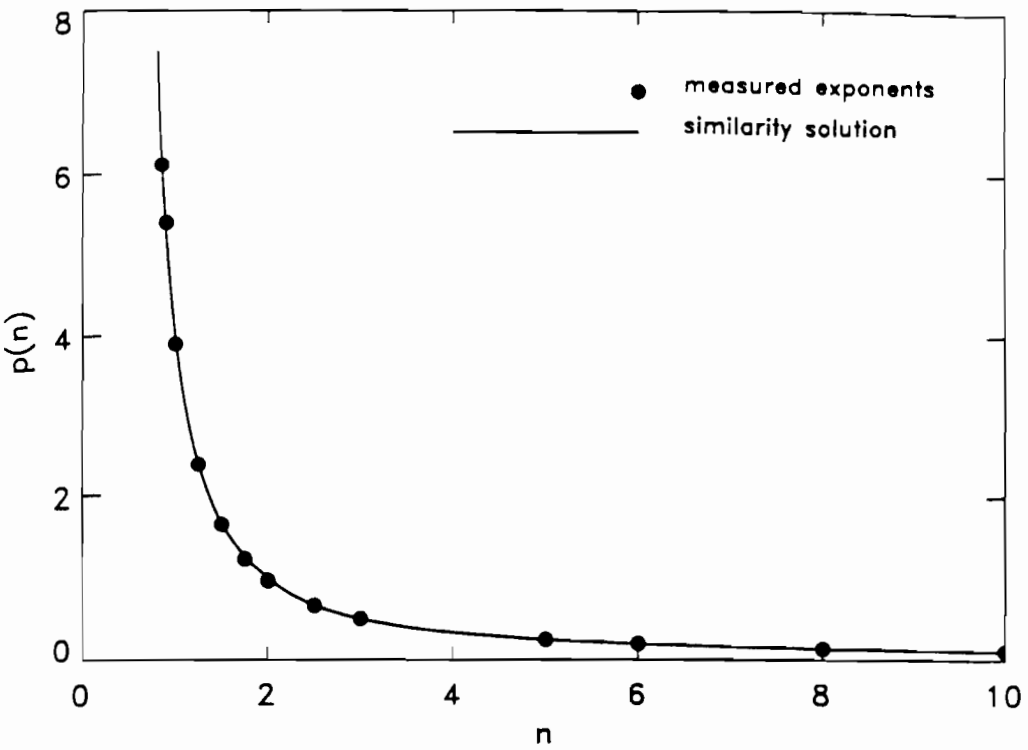

FIGURE 3.7. Exponent $p(n)$ of $h_{min} \sim t^{-p(n)}$ as a function of n. The measured exponents are compared with those of the similarity solution, equations (3.15a) and (3.15b). Error bars, as determined by the least squares fit, are typically ± 0.01. There is also a significant error which depends on the rate of convergence of the similarity solution.

show numerical results for the case $n = 1.1$. Figure 3.9 shows $h_{min}(t)$ as a function of $t_c - t$ and indicates that the singularity occurs in finite time. To illustrate that the pinch region obeys (3.18), in Figure 3.10 we show a plot of h_{xx} versus x at several different times close to the singular time for $n = 1.1$. Indeed, on the edges of the pinch region, h_{xx} approaches a constant value. Figure 3.11 shows a plot of $h(x,t)/h_{min}(t)$ as a function of $(x - x_p(t))/h_{min}^{1/2}$ for five different times, where we numerically compute $x_p(t)$ to satisfy $h(x_p(t),t) = h_{min}(t)$. The collapse of the data verifies the self-similar behavior of the solution. The solid line is a solution to the current equation with $H(0) = 1$, $H_\eta(0) = 0$, $H_{\eta\eta}(0) = 1.7$, and $\lambda = 0.5$. The agreement is excellent. We see roughly the same scaling behavior for solutions with $1.25 \gtrsim n \gtrsim 0.75$.

In order to completely understand this singularity we need to determine $h_{min}(t)$. This requires a complete match to the outer and central region. Dupont et al. [11] accomplished this for the $n = 1$ case. The corrections

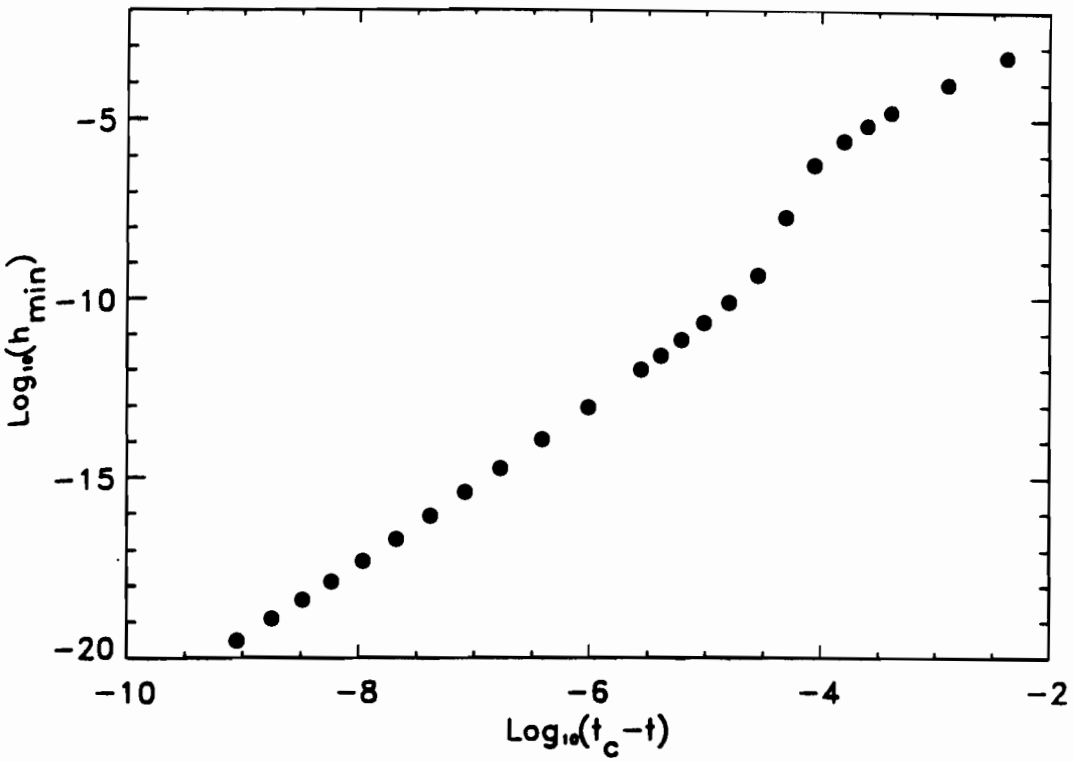

FIGURE 3.9. Time dependence of asymmetrical finite time singularities for $n = 1.1$. We show $\log(h_{min})$ versus $\log(t_c - t)$.

must go to zero in finite time, causing a singularity. For large n, the system forms singularities at the edge of the domain ($x = \pm 1$), as in the case of Figure 1.5. In our simulations, we observe that singularities form on the edge of the computational domain for $n > 2$. For $n < 1.5$, we never observe such an edge singularity. Our simulations are inconclusive as to whether the singularity forms in the interior or the edge for $1.5 < n < 2$.

The $n > 2$ edge singularities have a characteristic form. The minima of h, at $\pm x_p(t)$, progress to the boundary. For simplicity, we again consider the side close to the $x = 1$ boundary. Near the boundary but far from $x_p(t)$, $h(x,t)$ is a parabola:

$$h(x,t) = \frac{(x - x_p(t))^2}{(1 - x_p(t))^2} \quad \text{for} \quad 0 < \frac{x - x_p(t)}{1 - x_p(t)} \sim 1. \tag{3.20}$$

The current in the pinch [near $x_p(t)$] is quite small, and in fact goes to zero as $t \to t_c$. Hence, the current at the boundary, which is fixed by the boundary condition, controls the flow out of the region $[x_p, 1]$. For $t < t_c$,

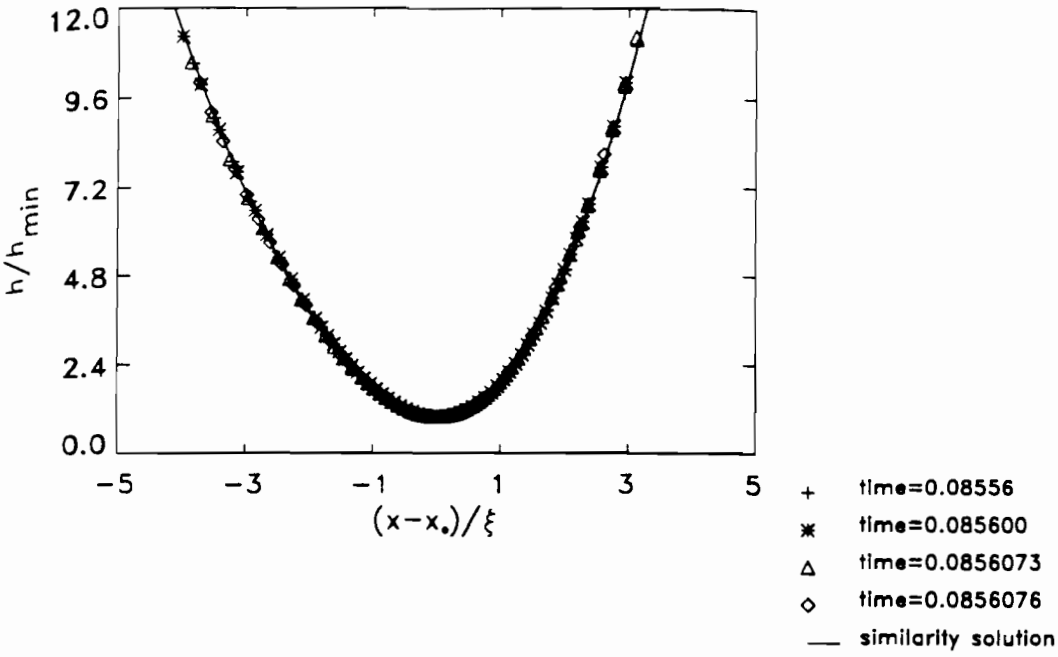

FIGURE 3.11. Rescaled profiles for the pinch region for $n = 1.1$. Each symbol represents a numerical solution at a different time. The solid line is a solution to the current equation, with $H(0) = 1$, $H_\eta(0) = 0$, and $H_{\eta\eta}(0) = 1.70$. The parameter $\lambda = 0.5$.

The matching to the outer region breaks down for $n < 3/2$, since equation (3.23) does not admit the asymptotic behavior $H \sim A\eta^2$ in this regime. This similarity solution can only describe singularity formation on the boundary for $n > 3/2$.

In order to complete the solution we must match to the central region. Recall in the case of infinite time singularities, the flux or current of fluid leaving the central region determines time dependences in the pinch region. Here the time dependence (3.25) follows from only the match to the boundary conditions. However, it is still true that the flux of fluid from the central region affects the solution. The neglect of this flux is only valid near the boundary, where the total flux is of order one [much larger than the flux from the central region, which is $O(\xi^s)$].

We verify that near the boundary, the similarity solution (3.23)–(3.24) holds. To check this we look at the specific case $n = 7.5$. We study the solution near $x^*(t)$, the maximum of h_{xxx}. The maximum x^* occurs to the right of x_p, the minimum of h. As $t \to t_c$, $h_{xxx}(x^*(t), t)$ diverges. Figure 3.12 shows the relation between $h_{xxx}(x^*(t), t)$ and $\xi(t)$. Figure 3.13 shows the dependence of $x^*(t)$ on $t_c - t$. Figure 3.14 shows the dependence of $h_{xxx}(x^*(t), t)$ on $t_c - t$. The solid line in each case shows the prediction of the similarity solution. The agreement is excellent. We also need to check

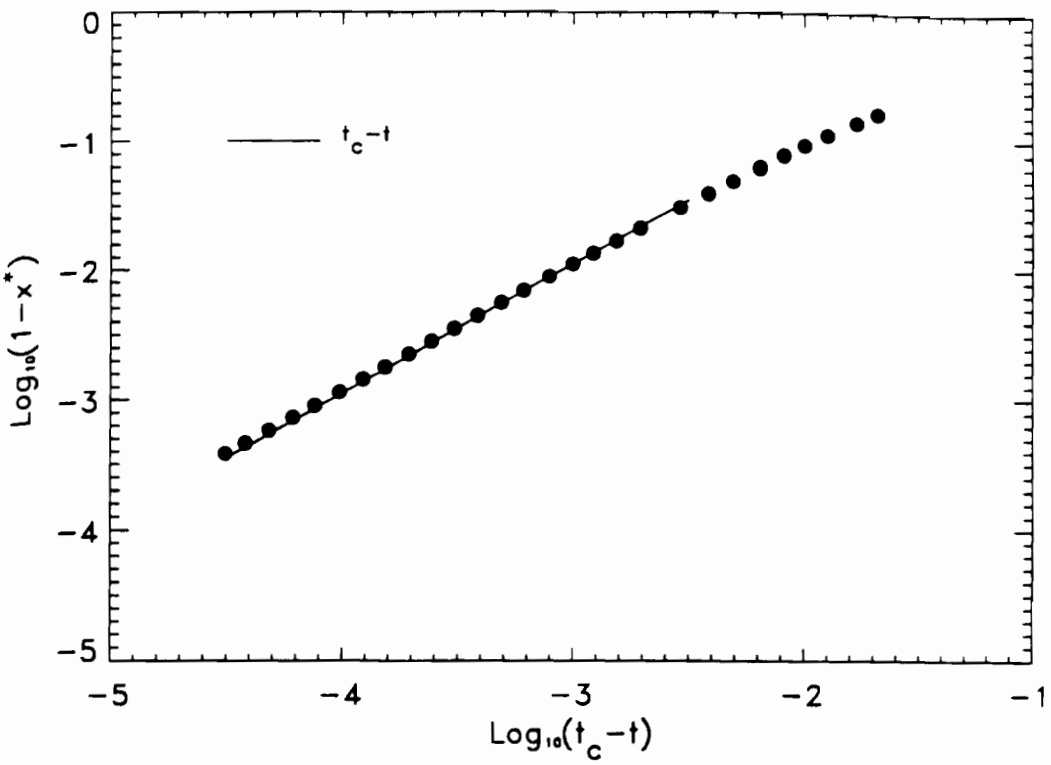

FIGURE 3.13. Dependence of $x^*(t)$ on $t_c - t$ for touchdown on the boundary, $n = 7.5$. The solid line gives the prediction of the theory.

determine the solution, for there are two exponentially growing solutions of the linearized (3.26) as $\eta \to -\infty$. The solution satisfying these conditions for $n = 7.5$ has $H(0) = 7.5/6.5$, $H_\eta(0) = 0.3542$, and $H_{\eta\eta}(0) = 0.7077$. In Figure 3.15 we compare this solution with results of a numerical simulation. In the upper half of the figure we show $h(x,t)/h_{xxx}(x^*(t))^{-1/6.5}$ versus $(x - x^*(t))/h_{xxx}(x^*(t))^{-7.5/19.5}$ for four different times. In the lower half of the figure we show $h_{xxx}(x,t)/h_{xxx}(x^*(t))$ versus $(x - x^*)/h_{xxx}(x^*(t))^{-7.5/19.5}$. The solid lines are the solutions described above. Indeed, the agreement between the similarity solution and the data is excellent up to the minimum of h, where the numerical data clearly deviate from the similarity solution. Beyond this point, the numerical data do not even collapse. Furthermore, there is an interesting dynamic structure in this region (not visible in Figure 3.15) that we defer until Section 6.4.

The similarity solution seems to agree with the numerics for a wide range of n. As an indication, in Figure 3.16 we show the scaling exponent $q(n)$ of $h_{xxx}(x^*,t) \sim \xi^{q(n)}$ as a function of n. In Figure 3.17 we show the scaling exponent $p(n)$ of $h_{xxx}(x^*,t) \sim (t_c - t)^{p(n)}$. The points represent the result of least squares fits to the data. The error in the points depends on how close the simulation is to t_c, the singular time. In each case, the solid line

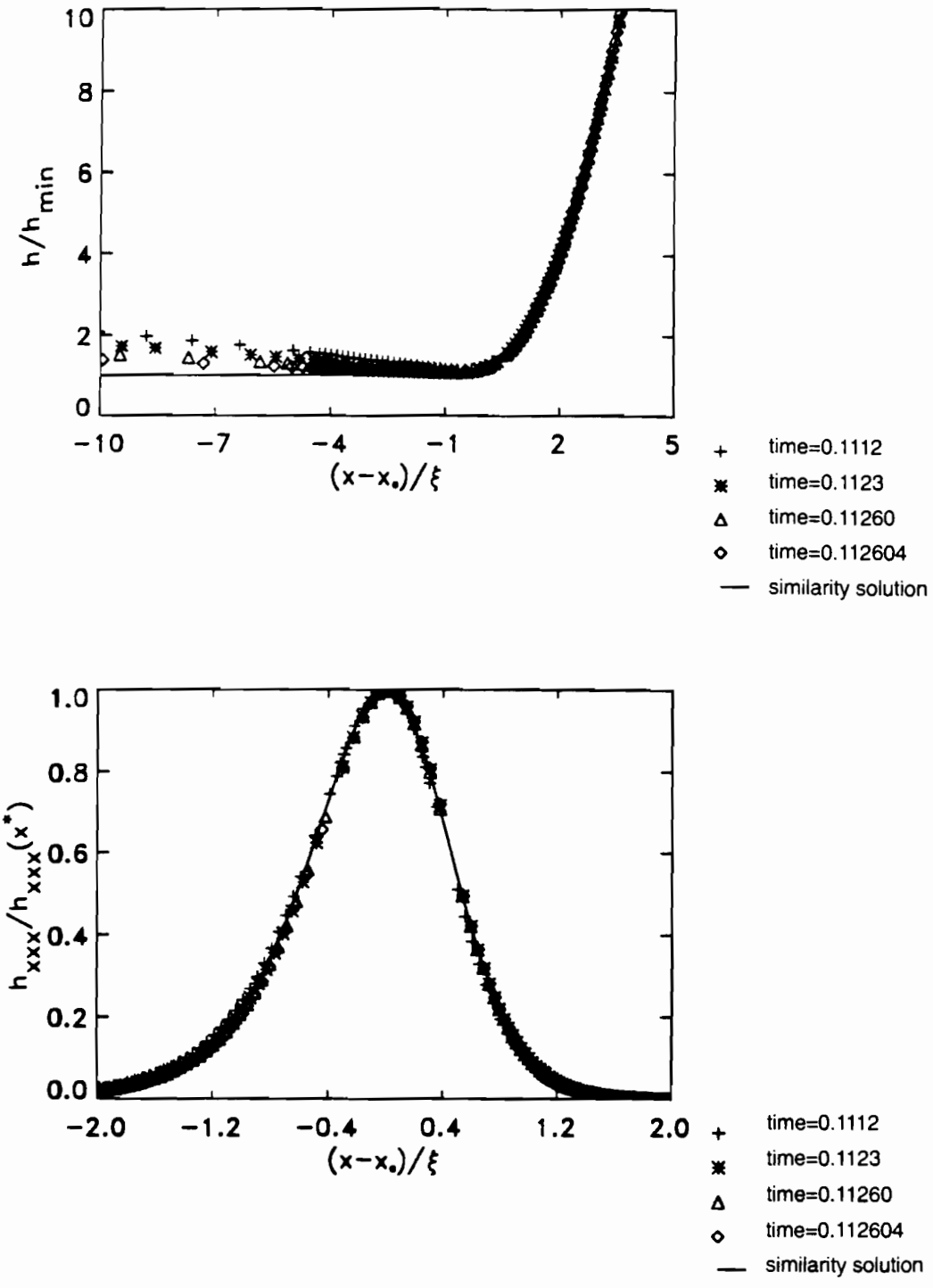

FIGURE 3.15. Rescaled profiles near the singularity for $n = 7.5$. The upper figure shows rescaled height profiles, and the lower figure shows rescaled h_{xxx} profiles. Each different symbol represents a numerical solution at a different time. The solid line is a solution to the velocity equation with initial conditions as described in the text. Notice that the scaling breaks down to the right of the minimum.

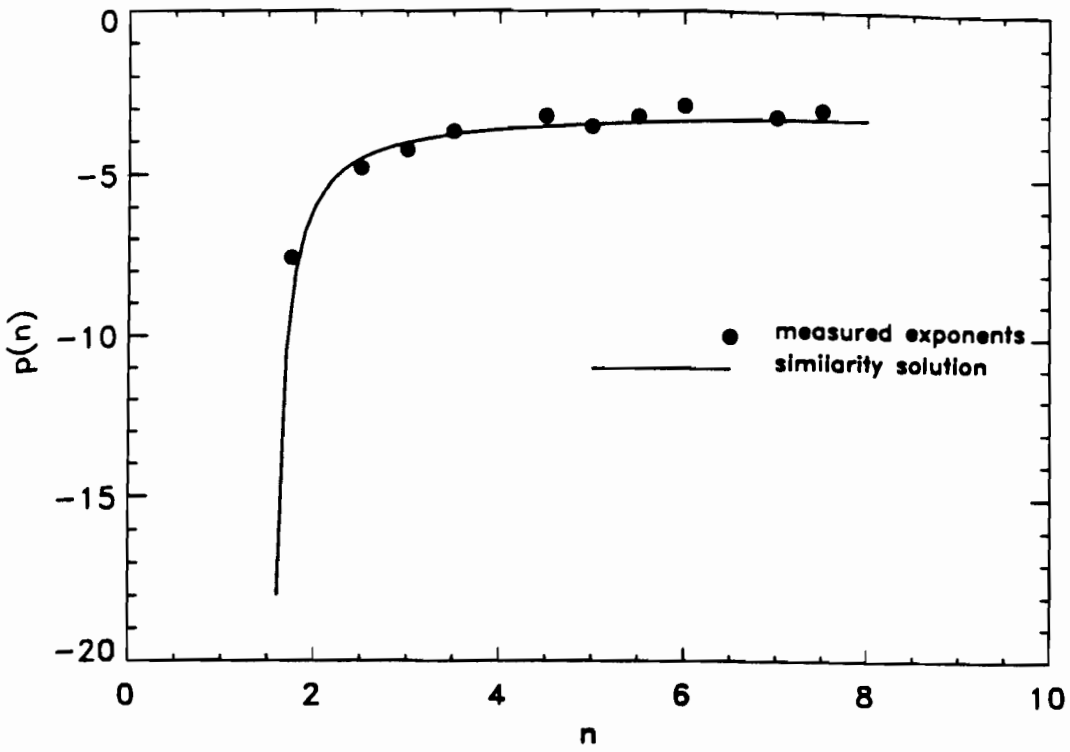

FIGURE 3.17. Exponent $p(n)$ of $h_{xxx}(x^*,t) \sim (t_c - t)^{p(n)}$ for boundary singularities with $n \geq 1.5$. The measured exponents are compared with those of the similarity solution.

Writing $h = H_0 + g$, g must satisfy

$$((H_0 + g)^n g_{xxx})_x = 1 \tag{3.29}$$

so that

$$g_{xxx} = \frac{x}{(g + H_0)^n}. \tag{3.30}$$

We formally expand equation (3.30) in powers of g. If $n < 1$, the successive terms in the expansion decrease for small $|x|$ and $|t_c - t|$.

The first-order correction to H_0 satisfies

$$g_{xxx} = \frac{x}{H_0^n}. \tag{3.31}$$

In Figure 3.18 we show the dependence of the minimum height, h_{min} on ξ, the characteristic width, for $n = 0.75$. In Figure 3.19 we show the dependence of h_{min} on $t_c - t$ for $n = 0.75$. In both cases, the solid lines represents the prediction of the similarity solution. The agreement is excellent. We also check that the the correction to H_0, which satisfies equation

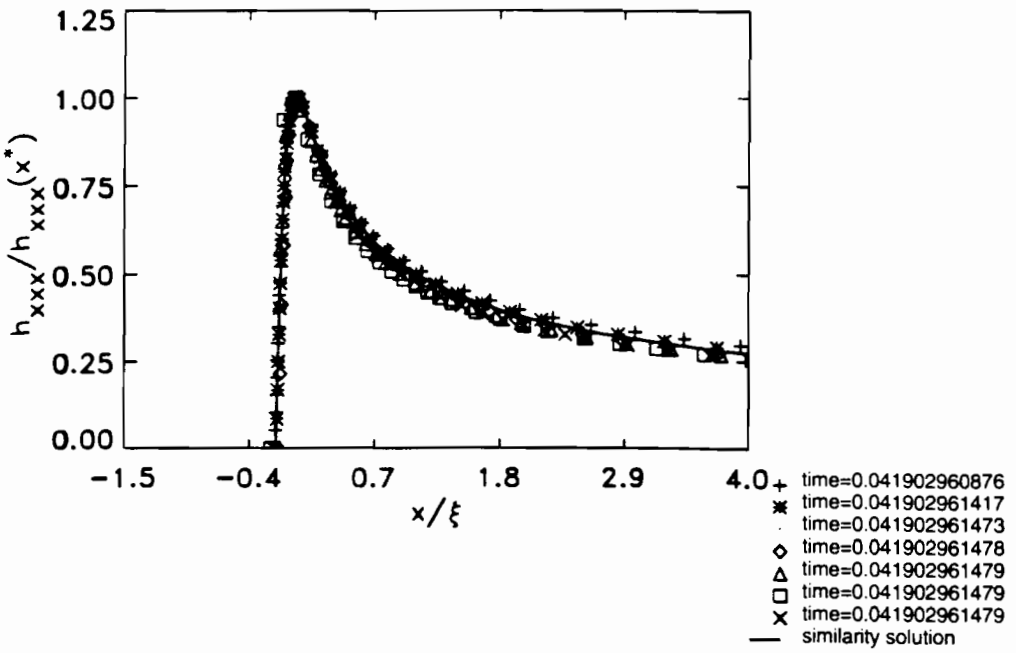

FIGURE 3.20. Rescaled h_{xxx} versus x profiles near the singularity for $n = 0.75$. Each symbol represents a numerical solution at a different time. The solid line is the first-order correction to the parabolic solution, as determined by equation (3.31).

(3.31), is present in the data. We can isolate the correction by examining h_{xxx}. For $n > 0.5$, h_{xxx} has a maximum at

$$x^* = \left(\frac{t_c - t}{B(2n-1)}\right)^{1/2}. \tag{3.32}$$

In Figure 3.20 we plot $h_{xxx}/h_{xxx}(x^*)$ versus $x/(h_{xxx}(x^*))^{-2}$ for seven different times at $n = 0.75$. The data collapse quite well. The solid line represents a solution (3.31) with $B = 69.2$ In Figure 3.21 we show a similar plot for $n = 0.25$. Here we plot $h_{xxx}(x,t)/h_{min}^{0.25}$ versus $x/h_{min}^{0.5}$ for seven different times. Again the data collapse; the agreement with the similarity solution $B = 2.5$ is excellent. We repeat this analysis for many values of n less than one, with similar agreement. As an example, in Figure 3.22 we show the exponent of $h_{min} \sim \xi^{q(n)}$ as a function of n. The solid line represents the prediction of the similarity solution, and the points are the results of simulations. In Figure 3.23 we show the exponent of $h_{min} \sim (t_c - t)^{p(n)}$ as a function of n, for both theory and simulations. Again the agreement is excellent.

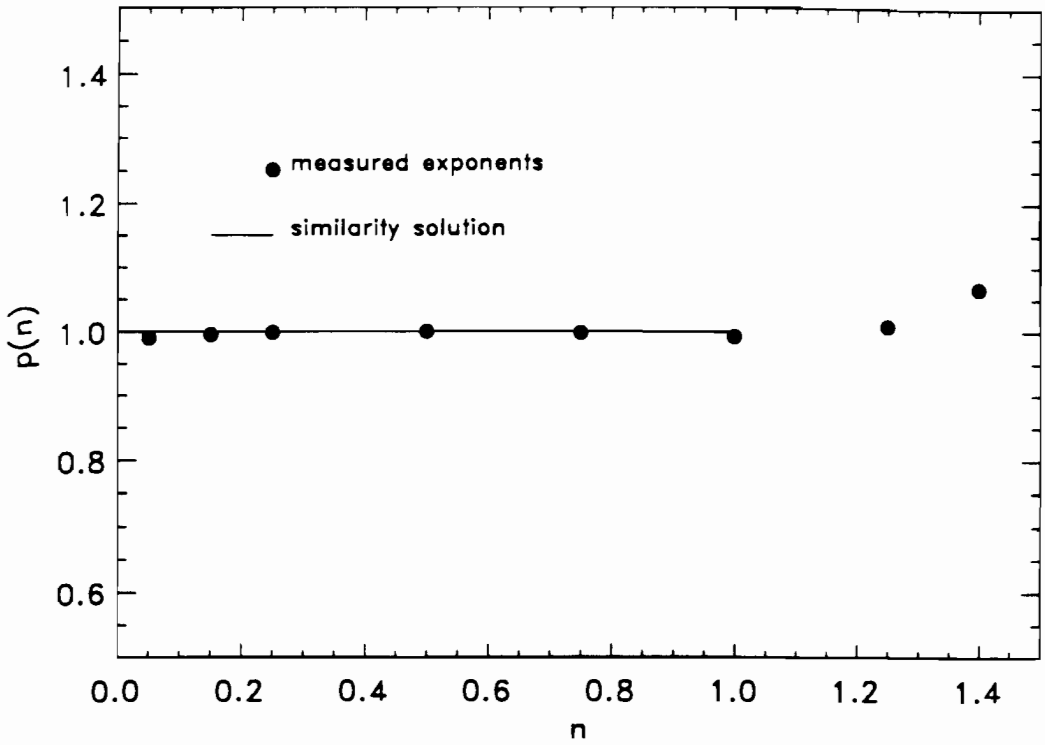

FIGURE 3.23. Exponent $p(n)$ of $h_{min} \sim (t_c - t)^{p(n)}$ for finite time touchdown at $x = 0$. The measured values are compared with the exponents of the similarity solution.

We also include in Figure 3.22 and 3.23 points for $n > 1$. Although it is possible (with a slight modification) to construct a similar expansion for $1 \leq n < 2$, such solutions do not agree with the measured exponents. Numerically we do not seem to observe this singularity all the way up to $n = 2$.

6.4 Unsolved Problems

6.4.1 Singularities and Similarity Solutions

In Section 6.3, we describe many singularities of the model equation (1.11) which exhibit self-similar structure. We compare the characteristics of these singularities to those of various similarity solutions that approximate the model equation. Our analysis is in the spirit of matched asymptotics, formulated for analyzing the solutions of ordinary differential equations [12]. In order for a similarity solution to describe the region around the singularity (the inner region) we must be able to match the solution to boundary

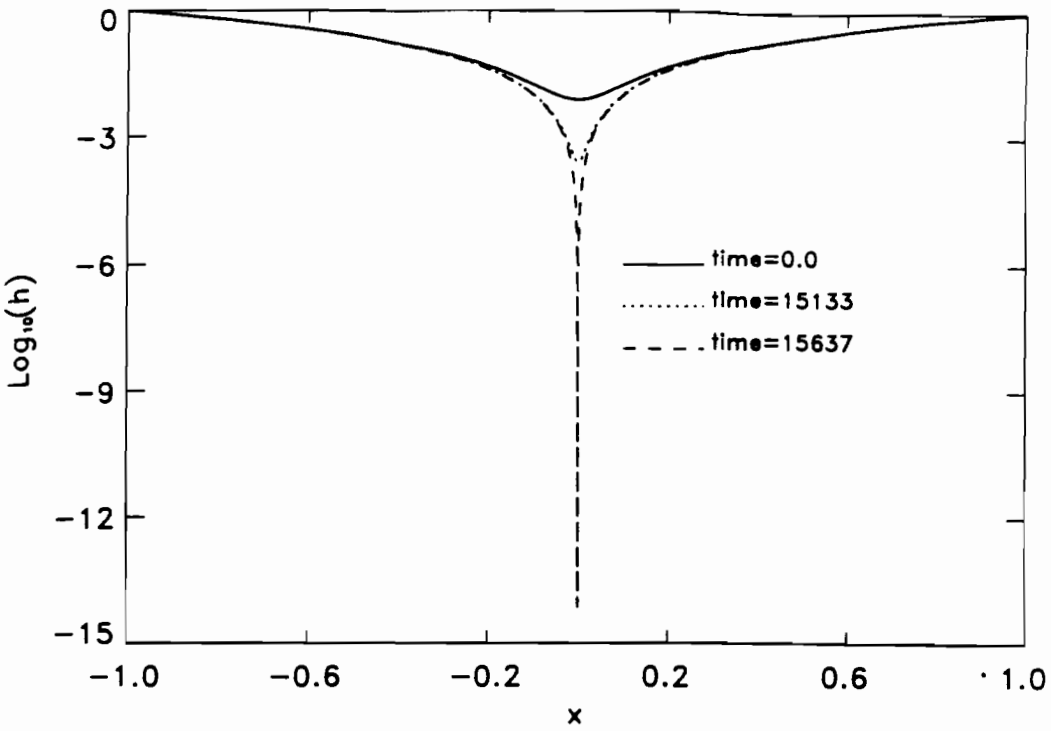

FIGURE 4.1. Early time structure of solution for $n = 1.6$. It appears that there will be a singularity at $x = 0$.

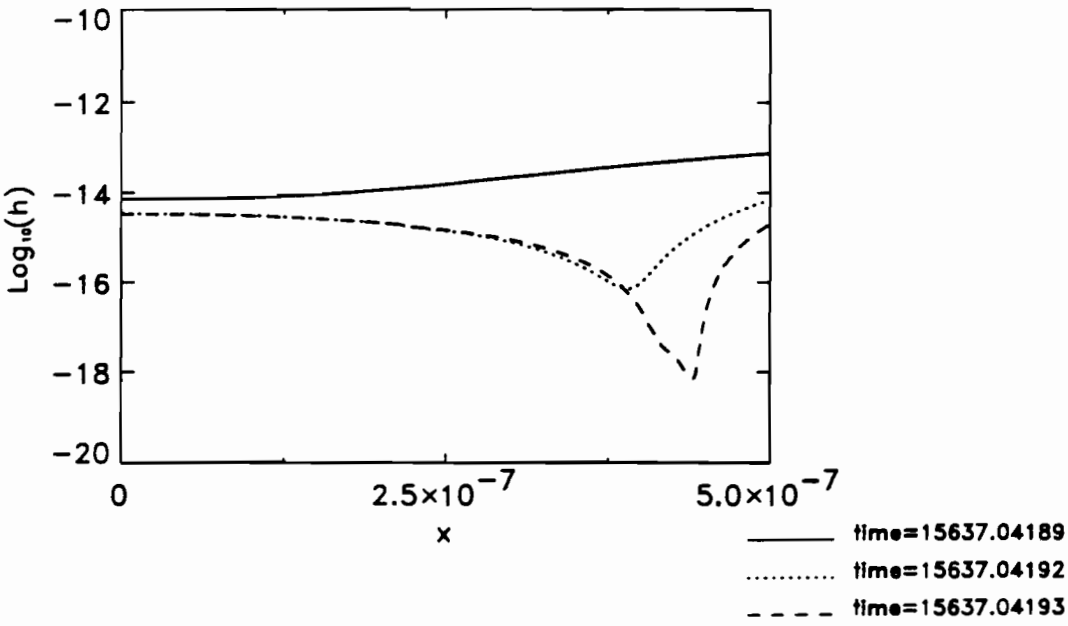

FIGURE 4.2. Blow-up of the preceding $n = 1.6$ solution at a slightly later time. The minimum is no longer at $x = 0$.

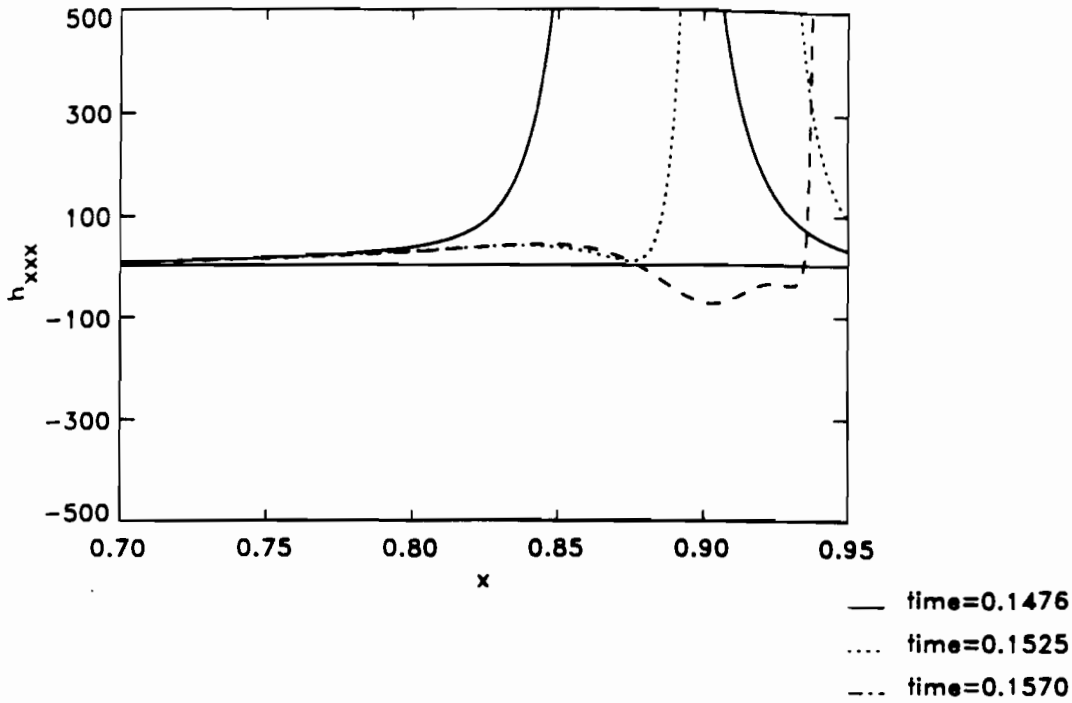

FIGURE 4.4. Numerical solution at the foot of the maximum of the h_{xxx} profile in the case of edge singularity for $n = 2.5$. Note the formation of a foot-like structure, as in the $n = 7.5$ case.

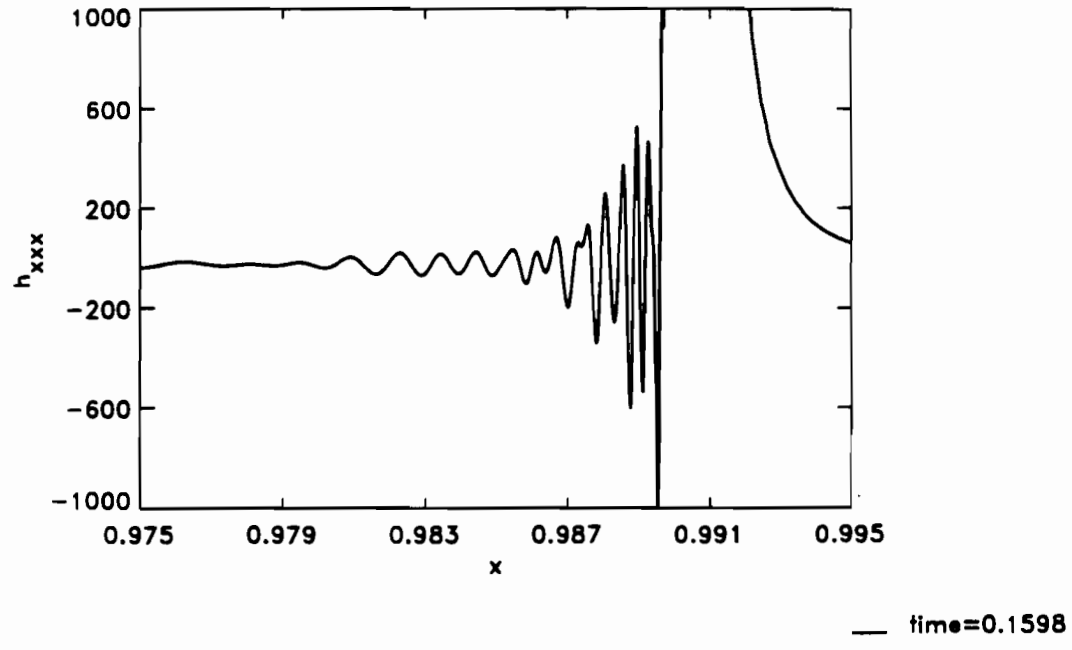

FIGURE 4.5. Numerical solution near the foot for $n = 2.5$ at a later time.

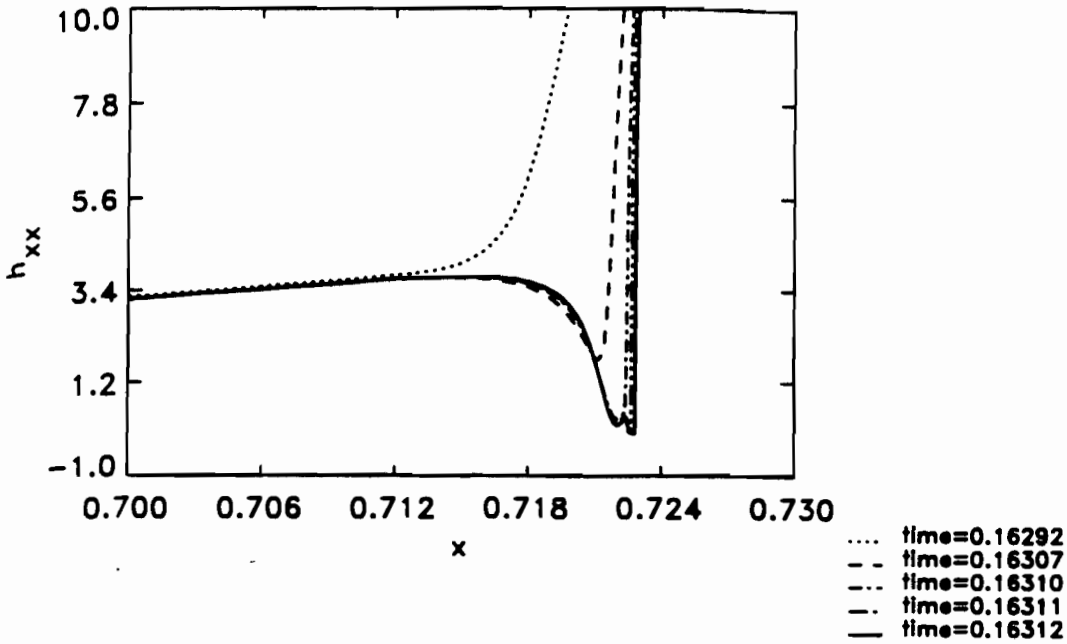

FIGURE 4.7. Blow-up of the previous figure. Notice the "tip" has the added structure of a smaller tip.

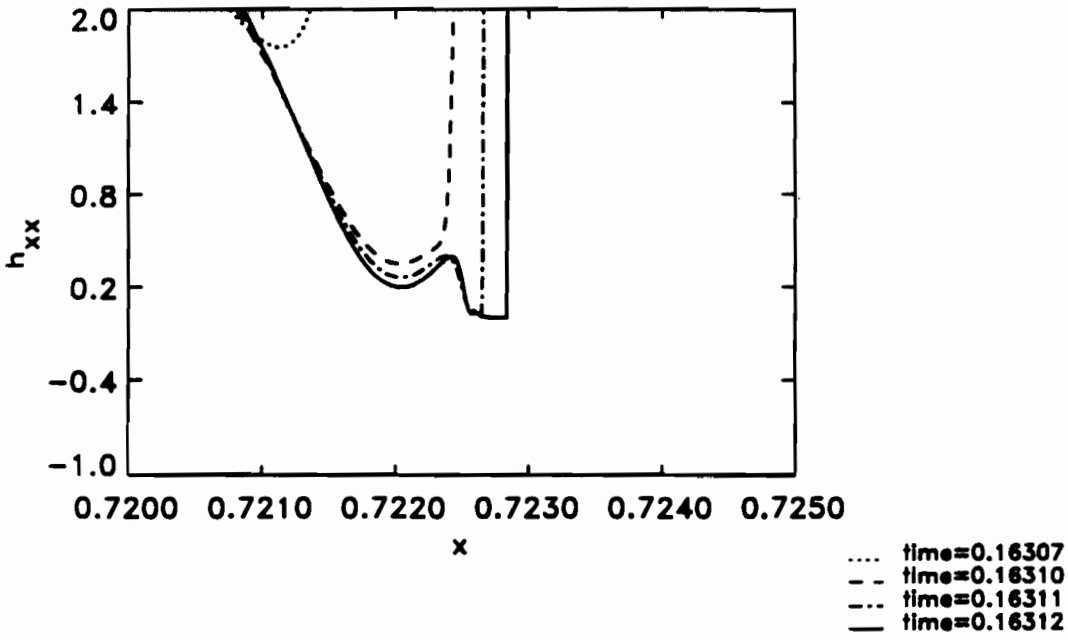

FIGURE 4.8. Blow-up of the "tip" region in the previous figure. The "tip" region also has a "tip".

[5] Stephanella Boatto, Leo Kadanoff, and Piero Olla, *Phys. Rev. E* **48**, 4423 (1993).

[6] M. Brenner and A. Bertozzi, On the spreading of droplets on a solid surface. *Phys. Rev. Lett.* **71**(4), 593–596 (1993).

[7] A. Cameron, *Principles of Lubrication.* Longmans, London, 1966.

[8] P. Constantin, T. Dupont, R. Goldstein, L. Kadanoff, M. Shelley, and S. Zhou, Droplet breakup in a model of the Hele–Shaw cell. *Phys. Rev. E* **47**(6), 4169–4181 (1993).

[9] P.G. de Gennes, Wetting: Statics and dynamics. *Rev. Mod. Phys.* **57**, 827–863 (1985).

[10] C. Domb and M.S. Green (eds.), *Phase Transitions and Critical Phenomena.* Academic Press, London, 1972.

[11] T. Dupont, R. Goldstein, L. Kadanoff, and S. Zhou, Finite-time singularity formation in Hele–Shaw systems. *Phys. Rev E* **47**(6), 4182–4196 (1993).

[12] M. Van Dyke, *Perturbation Methods in Fluid Mechanics.* Parabolic Press, Stanford, CA, 1975.

[13] J. Eggers and T.F. Dupont, Drop formation in a one-dimensional approximation of the Navier–Stokes equation. To appear, *J. Fluid Mech.*

[14] M.J. Shelley, R.E. Goldstein, and A.I. Pesci, Topological transitions in Hele–Shaw flow. In *Singularities in Fluids, Plasma, and Optics*, R.E. Caflisch and G.C. Papanicolou (eds.), pp. 167–188.

[15] R.E. Goldstein, A.I. Pesci, and M.J. Shelley, Topology transitions and singularities in viscous flows. *Phys. Rev. Lett.* **70**(20), 3043–3046 (1993).

[16] R.E. Goldstein, T.G. Mason, and E. Shyamsunder. Private communication.

[17] H.P. Greenspan, On the motion of a small viscous droplet that wets a surface. *J. Fluid Mech.* **84**, 125–143 (1978).

[18] D. Grier and N. Morgan. Private communication.

[19] L.M. Hocking, Sliding and spreading of this two-dimensional drops. *Quart. J. Mech. Appl. Math.* **34**, 37–55 (1981).

[20] Chun Huh and L.E. Scriven, Hydrodynamic model of steady movement of a solid/liquid/fluid contact line. *J. Colloid Interface Sci.* **35**, 85–101 (1971).